2568 *Chem. Mater.* **2009,** *21,* 2568–2570
DOI:10.1021/cm901273v

CHEMISTRY OF MATERIALS
Communication

Surfactant-Assisted Hydrothermal Synthesis of Single phase Pyrite FeS_2 Nanocrystals

Cyrus Wadia,[†,‡,▽] Yue Wu,[†,▽] Sheraz Gul,[⊥] Steven K. Volkman,[§] Jinghua Guo,[⊥] and A. Paul Alivisatos*[,†,∥,#]

[†]*Department of Chemistry and* [‡]*Energy & Resources Group and* [§]*Department of Electrical Engineering and Computer Sciences and* [∥]*Department of Materials Science and Engineering and University of California, Berkeley, California 94720,* [⊥]*Advanced Light Source and* [#]*Materials Science Division, Lawrence Berkeley National Laboratory, Berkeley, California 94720.* [▽] *These authors contributed equally to this work.*

Received May 7, 2009

Iron pyrite (FeS_2) has long been a material of interest for photovoltaic devices.[1] With an indirect energy transition at 0.95 eV, a direct transition at 1.03 eV,[1b] and an integrated absorption coefficient of 3.3×10^5 cm^{-1} for the energy spectrum of wavelength values (λ) between 300 and 750 nm, it is ideally suited for photovoltaic applications. This coupled with low procurement costs and vast abundance gives pyrite the potential to be a disruptive photovoltaic material when compared to many other candidates.[2] Numerous iron sulfides exist in nature, each with unique magnetic and electrical properties that are strongly related to the stoichiometric ratio between Fe and S as well as crystalline structure. Pyrite has previously been prepared using several high temperature approaches including MOCVD, sulfurization of iron films, sulfurization of iron oxide films, reactive sputtering, and spray pyrolysis,[3,1b] yet at elevated temperatures, segregation of iron and sulfur species is unavoidable, which could change the stoichiometry and material phase of the deposited film. In fact, the best demonstrated pyrite photovoltaic device by these techniques shows a modest 2.8% power conversion efficiency.[1a] This low performance was partially explained by a high density of surface defects, but the unusually low open circuit voltage of 200 mV suggests that phase purity may also play a role.[1,3] Orthorhombic marcasite FeS_2 and hexagonal troilite FeS are both common iron sulfur phases, but because they have much smaller band gaps (0.34 eV for marcasite and 0.04 eV for troilite), even trace amounts would explain the low open circuit voltage observed in this previous work.

Semiconductor nanocrystals have been used as building blocks to assemble a range of electronic and photonic structures, including light emitting diodes, lasers, and photovoltaics.[4] Critical to the functionality of these types of devices are the purity, crystallinity, stoichiometry, and size of the nanocrystal building blocks. While some low temperature solution phase colloidal nanocrystal synthesis approaches to pyrite have been explored,[5] these efforts are early, and unlike their thin film predecessors, there are no reports on photovoltaics made from these synthetic materials.

Single source molecular precursors with precisely defined composition can provide a high degree of control of nanocrystal synthesis, as demonstrated with the growth of CdS, ZnS, CdSe, ZnSe, Sb_2Te_3, and In_2S_3 nanocrystals[6] as well as the growth of CdS and ZnS nanowires.[7] Herein, we report the use of single-source molecular precursors for the growth of single phase FeS_2 pyrite nanocrystals through a hydrothermal reaction. Surfactant selection and control of solution pH have been found to play key roles in the preparation of single phase iron pyrite.

Our synthetic approach starts with the formation of the single source molecular precursor iron(III) diethyl dithiophosphate ($[(C_2H_5O)_2P(S)S]_3Fe$) in aqueous solution through the reaction between iron(III) chloride ($FeCl_3$) and diethyl dithiophosphate ammonium salt ($((C_2H_5O)_2P(S)SNH_4$) (formation of this product was confirmed through mass spectrometry studies and is detailed in the

(1) (a) Ellmer, K.; Tributsch, H. Iron Disulfide (Pyrite) as Photovoltaic Material: Problems and Opportunities; Proceedings of the 12th Workshop on Quantum Solar Energy Conversion, Wolkenstein, Sudtirol, Italy, May 11−18, 2000; The European Society for Quantum Solar Energy Conversion: Wolkenstein, Sudtirol, Italy, 2000. (b) Ennaoui, A.; Fiechter, S.; Pettenkofer, C.; Alonsovante, N.; Buker, K.; Bronold, M.; Hopfner, C.; Tributsch, H. Sol. Energy Mater. Sol. Cells **1993**, 29(4), 289–370. (c) Altermatt, P.; Kiesewetter, T.; Ellmer, K.; Tributsch, H. Sol. Energy Mater. Sol. Cells **2002**, 71(2), 181–195. (d) Chatzitheodorou, G.; Fiechter, S.; Konenkamp, R.; Kunst, M.; Jaegermann, W.; Tributsch, H. Mater. Res. Bull. **1986**, 21(12), 1481–1487. (e) Ennaoui, A.; Tributsch, H. Sol. Cells **1984**, 13(2), 197–200. (f) Ennaoui, A.; Tributsch, H. Sol. Energy Mater. **1986**, 14(6), 461–474. (g) Nesbitt, H. W.; Bancroft, G. M.; Pratt, A. R.; Scaini, M. J. Am. Mineral. **1998**, 83, 1067–1076.
(2) Wadia, C.; Alivisatos, A. P.; Kammen, D. *Environ. Sci. Technol.* **2009**, 43(6), 2072–2077.
(3) Luther, G. *Geochim. Cosmochim. Acta* **1991**, 55(10), 2839–2849.
(4) (a) Coe, S.; Woo, W. K.; Bawendi, M.; Bulovic, V. *Nature* **2002**, 420 (6917), 800–803. (b) Klimov, V. I.; Mikhailovsky, A. A.; Xu, S.; Malko, A.; Hollingsworth, J. A.; Leatherdale, C. A.; Eisler, H. J.; Bawendi, M. G. Science **2000**, 290(5490), 314–317. (c) Sun, S. H.; Murray, C. B. J. Appl. Phys. **1999**, 85(8), 4325–4330. (d) Huynh, W. U.; Dittmer, J. J.; Alivisatos, A. P. Science **2002**, 295(5564), 2425–2427.
(5) (a) Chen, X. H.; Fan, R. *Chem. Mater.* **2001**, 13(3), 802–805. (b) Chen, X. Y.; Wang, Z. H.; Wang, X.; Wan, J. X.; Liu, J. W.; Qian, Y. T. Inorg. Chem. **2005**, 44(4), 951–954. (c) Duan, H.; Zheng, Y. F.; Dong, Y. Z.; Zhang, X. G.; Sun, Y. F. Mater. Res. Bull. **2004**, 39(12), 1861–1868. (d) Kar, S.; Chaudhuri, S. Chem. Phys. Lett. **2004**, 398(1−3), 22–26. (e) Kar, S.; Mandal, S. K.; Das, D.; Chaudhuri, S. Mater. Lett. **2004**, 58(22−23), 2886–2889. (f) Xuefeng, Q.; Xie, Y.; Yitai, Q. Mater. Lett. **2001**, 48, 109–111.
(6) (a) O'Brien, P.; Walsh, J. R.; Watson, I. M.; Hart, L.; Silva, S. *J. Cryst. Growth* **1996**, 167(1−2), 133–142. (b) Cumberland, S. L.; Hanif, K. M.; Javier, A.; Khitrov, G. A.; Strouse, G. F.; Woessner, S. M.; Yun, C. S. Chem. Mater. **2002**, 14(4), 1576–1584. (c) Crouch, D. J.; O'Brien, P.; Malik, M. A.; Skabara, P. J.; Wright, S. P. Chemical Commun. **2003**, No. 12, 1454–1455. (d) Revaprasadu, N.; Malik, M. A.; O'Brien, P.; Zulu, M. M.; Wakefield, G. J. Mater. Chem. **1998**, 8(8), 1885–1888. (e) Garje, S. S.; Eisler, D. J.; Ritch, J. S.; Afzaal, M.; O'Brien, P.; Chivers, T. J. Am. Chem. Soc. **2006**, 128(10), 3120–3121. (f) Afzaal, M.; Crouch, D.; Malik, M. A.; Motevalli, M.; O'Brien, P.; Park, J. H. J. Mater. Chem. **2003**, 13(4), 639–640.
(7) Barrelet, C. J.; Wu, Y.; Bell, D. C.; Lieber, C. M. *J. Am. Chem. Soc.* **2003**, 125(38), 11498–11499.

 Published on Web 06/16/2009

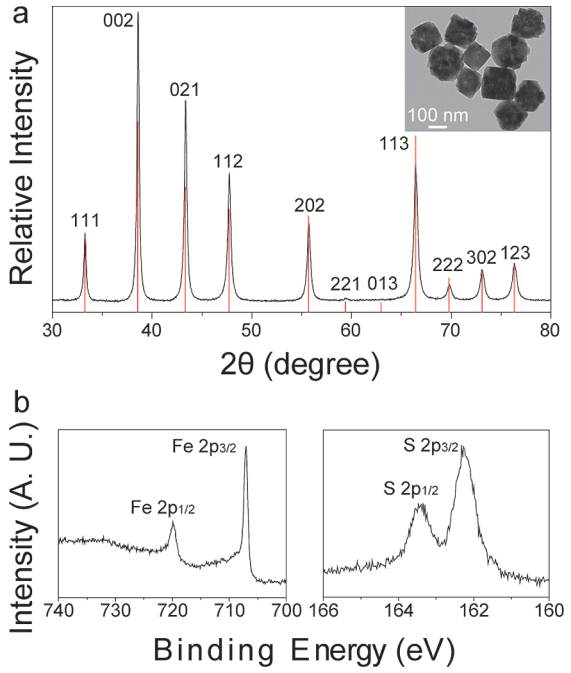

Figure 1. (a) XRD pattern and TEM image and (b) XPS spectra of pure pyrite FeS_2 yielded from hydrothermal synthesis.

Supporting Information). Then, the single source precursor with the addition of hexadecyltrimethylammonium bromide (CTAB) acting as a surfactant undergoes thermal decomposition by a hydrothermal reaction in a 125 mL Teflon lined stainless steel acid digestion bomb at 200 °C. We also demonstrate an alternative approach where the molecular precursor may be formed in situ and is detailed in the Supporting Information.

XRD studies (Figure 1a) show the materials prepared in this way are cubic pyrite FeS_2 (JCPDS 03-065-1211, Figure 1a red lines) without any noticeable impurity peaks from orthorhombic marcasite FeS_2 or hexagonal troilite FeS. Transmission electron microscopy (TEM) studies (inset, Figure 1a) show large quasi-cubic nanocrystal agglomerations with an average size over 100 nm. The pyrite nanocrystals were further investigated through X-ray photoelectron spectroscopy (XPS) (Figure 1b). Iron peaks in the XPS spectrum are associated with FeS_2. The Fe $2p_{3/2}$ binding energy of 707 eV (Figure 1b, left panel) is characteristic of pyrite (with no observable impurities from troilite). The S $2p_{3/2}$ and S $2p_{1/2}$ peaks at 162.28 and 163.47 eV, respectively (Figure 1b, right panel), are also consistent with the sulfur binding energy in bulk pyrite.[1g]

To elucidate their electronic structure, the FeS_2 nanocrystals have been studied by X-ray absorption spectroscopy (XAS) and X-ray emission spectroscopy (XES). XAS probes the local unoccupied electronic structure (conduction band); XES probes the occupied electronic structure (valence band); and the addition of resonant inelastic X-ray scattering (Raman spectroscopy with

(8) Guo, J. X-ray Absorption and Emission Spectroscopy in Nanoscience and Lifesciences. In Nanosystem characterization Tools in the Life Sciences; Kumar, C., Ed.; Wiley-VCH Verlag GmbH & Co. KgaA: Weinheim, 2006; pp 259−291.

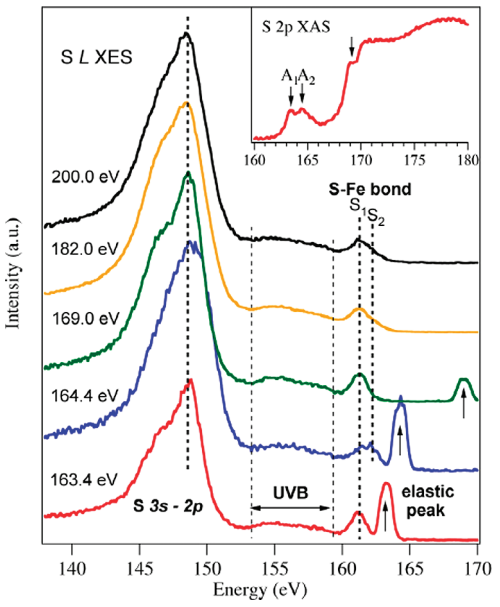

Figure 2. X-ray absorption spectrum of nanostructured FeS_2 (inset) and resonant excited X-ray emission spectra of S L-edges with the excitation energy indicated by the notations and arrows in the XAS spectrum.

X-rays) can provide significant insight into the energy levels that reflect the chemical and physical properties of semiconductors.[8] The experiment was performed on BL7 at the Advanced Light Source, Lawrence Berkeley National Laboratory. The resolution was set to 0.1 eV for XAS and 0.2 eV for XES.

The X-ray absorption and emission spectra of nanostructured iron pyrite were recorded at the S L-edge and Fe L-edge. The S 2p XAS spectrum (Figure 2, inset) reflects the density of states of the conduction band. The spin orbit splitting of about 1.2 eV is also reflected in the XAS spectrum, indicated as A1 and A2. The nonresonant excited S L-edge XES spectrum (Figure 2) shows the density of states of the valence band. The intensive band around 145−150 eV arises predominantly from levels with 3s character, while the upper valence band (UVB) being mostly of 3p character shows a much weaker intensity due to the dipole selection rule of the XES process. The small band close to the Fermi level at around 161 eV is attributed to S 3d states that are hybridized with Fe 3d states. Its asymmetric shape indicates the two components due to the valence states projected on L shell vacancies with spin orbital splitting of 1.2 eV for $2p_{3/2}$ and $2p_{1/2}$. When resonantly exciting A1 and A2 in the XAS spectrum, one can see the resonant enhancement for each corresponding component S1 and S2.

To determine the bandgap from the valence band maximum (VBM) to the conduction band minimum (CBM), we plot the resonantly excited S L-edge XES spectrum (excited at 169 eV) together with S 2p XAS spectrum (Figure 3a). The bandgap is 0.95 ± 0.1 eV as indicated in the figure. Resonant X-ray emission spectroscopy has also been used to determine the direct or indirect bandgap of semiconductors.[9] In a simplified

(9) Eisebitt, S.; Luning, J.; Rubensson, J. E.; Eberhardt, W. *Phys. Status Solidi B* **1999**, 215(1), 803–808.

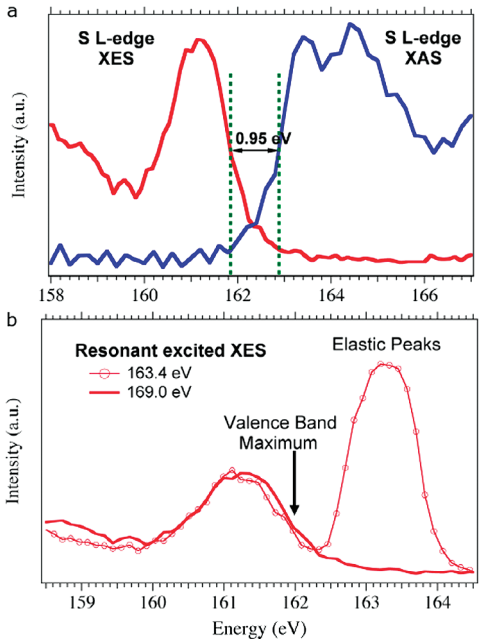

Figure 3. (a) Top of the valence band and bottom of the conduction band indicating the bandgap of 0.95 eV; (b) the shift of the top of the valence band from resonantly excited XES spectra suggesting an indirect bandgap in nanostructured FeS_2.

picture, one can say that the position of the electron in the CB band structure after the XAS event will select which VB electrons can participate in the XES process. The experimental handle to access band structure information is the excitation energy. Figure 3b shows that emission at the highest energy is not obtained for excitation at threshold, which suggests an indirect bandgap in the nanostructured FeS_2.

To gain further insight into the mechanisms and nature of our synthesis, a number of synthetic variations were performed (see Supporting Information). These variants included reaction temperature, reaction time, solution pH, and surfactants (primary, secondary, or tertiary mixtures). Slightly acidic conditions and the presence of a halogenated cetrimonium were critical in the formation of the pure phase of pyrite. Other parameters, including reaction time and cosurfactant, have been found to have little effect on the purity. Notably, when long chain alkylamines, for example, oleylamine, are used as a cosurfactant, smaller and more cubic-shaped nanocrystals can be obtained but at the expense of purity in which XRD patterns begin to show marcasite peaks. A detailed reaction mechanism is still under investigation.

In conclusion, we have demonstrated a single-source molecular precursor that can be used for the synthesis of single phase pyrite FeS_2 nanocrystals. Characterization confirms an indirect transition and a bandgap of 0.95 eV. The reaction temperature, pH value, precursor, and surfactant have been found to play important roles in the control of material purity. These single phase pyrite FeS_2 nanocrystals represent a good candidate material for studies of nanoscale photovoltaic solar cells based on nontoxic and earth abundant materials.

Acknowledgment. We thank Timothy Teague, Wanli Ma, Jonathan S. Owen, Michael Geier, Elena Schevchenko, and Dmitri Talapin for helpful discussions. C.W. thanks the Environmental Protection Agency for the EPA STAR Fellowship. Y.W. thanks the Miller Institute for Basic Research in Science for Miller Research Fellowship. This work was supported by the Director, Office of Science, Office of Basic Energy Sciences, Materials Sciences and Engineering Division, of the U.S. Department of Energy under Contract No. DE-AC02-05CH11231.

Supporting Information Available: Detailed procedures about experiments, molecular structure and mass spectrum of the molecular precursor, XPS spectrum of the pyrite FeS_2 nanocrystals, and TEM images of nanocrystals containing marcasite impurities synthesized using CTAB and oleylamine mixture (PDF). This material is available free of charge via the Internet at http://pubs.acs.org.